symmetry

MDPI

*Article*

# Constraints on Cosmic Ray Acceleration Capabilities of Black Holes in X-ray Binaries and Active Galactic Nuclei

**Arman Tursunov [1,2,3,*], Martin Kološ [1] and Zdeněk Stuchlík [1]**

1 Research Centre for Theoretical Physics and Astrophysics, Institute of Physics, Silesian University in Opava, Bezručovo nám. 13, CZ-74601 Opava, Czech Republic; martin.kolos@physics.slu.cz (M.K.); zdenek.stuchlik@physics.slu.cz (Z.S.)
2 Bogoliubov Laboratory of Theoretical Physics, Joint Institute for Nuclear Research, Joliot-Curie 6, 141980 Dubna, Russia
3 Institute of Experimental and Theoretical Physics, Al-Farabi Kazakh National University, Almaty 050040, Kazakhstan
* Correspondence: arman.tursunov@physics.slu.cz

**Abstract:** Rotating black holes (BHs) are likely the largest energy reservoirs in the Universe as predicted by BH thermodynamics, while cosmic rays (CRs) are the most energetic among particles detected on Earth. Magnetic fields surrounding BHs combined with strong gravity effects, thanks to the spacetime symmetries, turn the BHs into powerful accelerators of charged particles. At the same time, in the age of multi-wavelength and multi-messenger astronomy, BHs and their environments have not yet been probed with CR messengers, despite being observed across most of the electromagnetic spectrum, and neutrino and gravitational waves. In this paper, we probe the acceleration capabilities of BHs in 8 galactic X-ray binaries and 25 local active galactic nuclei (AGNs) within 100 Mpc, based on the ultra-efficient regime of the magnetic Penrose process of a BH energy extraction combined with observational data. We find that the maximum energy of the galactic BHs can reach only up to the knee of the CR spectrum, including supermassive BH Sgr A* at the Galactic Center. On the other hand, for supermassive BHs in AGNs, we find that the mean energy of primary CRs is of the order of $10^{19}$ eV. It is therefore likely that local supermassive BHs give sufficient contribution to the ankle—a sharp change in the slope of the cosmic ray spectrum around $10^{18.6}$ eV energy. We also discuss the energy losses of primary CRs close to the acceleration zones. In the galactic BH cases, it is likely dominated by synchrotron radiation losses.

**Keywords:** cosmic rays; UHECR; black hole; AGN; GBH; GZK cutoff; magnetic field



**Citation:** Tursunov, A.; Kološ, M.; Stuchlík, Z. Constraints on Cosmic Ray Acceleration Capabilities of Black Holes in X-ray Binaries and Active Galactic Nuclei. *Symmetry* **2022**, *14*, 482. https://doi.org/10.3390/sym14030482

Academic Editor: Grant J. Mathews

Received: 27 January 2022
Accepted: 23 February 2022
Published: 26 February 2022



## 1. Introduction

Cosmic rays (CRs) are high-energy charged particles (primarily protons) moving through the Universe with enormous velocities; when hitting Earth's atmosphere, they produce air showers of secondary particles, allowing their detection at the surface. The highest energy CRs are usually referred to as ultra-high-energy cosmic rays (UHECRs), whose energy can even exceed $10^{20}$ eV. At energies exceeding $10^{18}$ eV, UHECRs are likely extragalactic, which is indicated by the anisotropy studies of the arrival directions of primary CR particles [1]. At lower energies, the spectrum has two knees at $10^{15.5}$ eV (the sharp one, considerably lowering the flux) and at about $10^{17.5}$ eV. While UHECRs at the highest energies are extragalactic, the origin of CRs above the knee still remain under debate. At higher energies, the spectrum attributes the ankle, showing a flattening of the spectrum at energies around $10^{18.6}$ eV. Interactions of high-energy protons (at energies above $\sim 10^{19.5}$ eV) during propagation along the large distances exceeding 100 Mpc with the cosmic microwave background photons put the limit on the maximum arrival energy of primary cosmic ray protons [2]. This prediction of the standard model of particle physics is known as the GZK cutoff [3,4]. Detection of CRs with energies greater than the GZK-cutoff limit in both hemispheres may either indicate the lack of our understanding of CR propagation scenarios, or the necessity of searches of powerful extragalactic CR accelerators within 100 Mpc distance.

Many attempts have been made to explain the origin of the UHECRs, which can be generally divided into exotic and acceleration scenarios. The latter are typically predicted on the presence of powerful cosmic objects with adequate energy to accelerate the CR particles. Among the prime targets are, for example, supernovae [5], active galactic nuclei [6] and blazars [7]. The shock acceleration in relativistic jets is among long-standing astrophysical scenarios [8]. Another acceleration model was recently proposed [9], which attempts to explain UHECRs by the extraction of energy from rotating supermassive black holes (SMBH) through the so-called magnetic Penrose process. The model is claimed to operate in a realistic astrophysical environment and constrains the SMBH mass and magnetic field strength in its vicinity for given UHECR energy. It also does not require neither an extended acceleration zone, nor fine-tuning of the parameters of matter accreting into SMBH. In this paper, we extend our previous studies related to supermassive BHs [9] to stellar mass BHs. Using the available observational data, we constrain the energy of primary CRs originated from X-ray binary systems containing stellar mass BHs and compare the results with those related to SMBH. Overall, we examine the CR acceleration capabilities of selected 8 galactic BH binaries and 25 AGN.

The paper is organized as follows. In Section 2, we give a brief description of the BH thermodynamics, extractable energy and BH magnetosphere based on the theoretical and observational results available in the literature. Using the measurements of masses and magnetic fields of three dozen galactic and extragalactic BH candidates, we find a heuristic formula for their magnetic field–mass relation. In Section 3, we present the CR acceleration model and put constraints on the maximal energy of CRs originated from a particular source. We summarize the results in the table and conclude the paper in Section 4.

## 2. Astrophysical Black Holes: Rotating and Magnetized

Multiwavelength and multimessenger studies of stellar mass and supermassive BH candidates provide no conclusive evidence of spacetime deviations from those of the Kerr metric. Given the precision of available instruments and their measurements, any astrophysical BH can be well characterized by only two parameters: mass $M$ and spin $a$. Therefore, further in this paper, by BH we shall mean the compact objects, whose metric is described by the rotating Kerr solution to the Einstein field equations. The Kerr metric reads

$$ds^2 = g_{tt}dt^2 + 2g_{t\phi}dtd\phi + g_{rr}dr^2 + g_{\theta\theta}d\theta^2 + g_{\phi\phi}d\phi^2, \tag{1}$$

where the metric tensor has the following non-zero components in the standard Boyer–Lindquist coordinates

$$\begin{aligned} g_{tt} &= -\left(1 - \frac{2Mr}{\Sigma}\right), \quad g_{t\phi} = -\frac{2Mra\sin^2\theta}{\Sigma}, \quad g_{rr} = \frac{\Sigma}{\Delta}, \\ g_{\theta\theta} &= \Sigma, \quad g_{\phi\phi} = \left(r^2 + a^2 + \frac{2Mra^2}{\Sigma}\sin^2\theta\right)\sin^2\theta, \\ \Sigma &= r^2 + a^2\cos^2\theta, \quad \Delta = r^2 - 2Mr + a^2. \end{aligned} \tag{2}$$

The ring at $r = 0$, $\theta = \pi/2$ defines the physical singularity, while the event horizon (outer) is given by

$$r_+ = M + (M^2 - a^2)^{1/2}. \tag{3}$$

The metric is unaffected by the existence of an external magnetic field, which is explained later in the paper.

### 2.1. Energy Extraction from Black Holes

According to the second law of BH thermodynamics [10], the rotational energy of BHs can in principle be extracted out, i.e., converted into accelerated particle energy. The dependence of the extractable rotational energy $E_{\rm rot}$ on the spin parameter of the BH reads

$$E_{\rm rot} = Mc^2 \left[ 1 - \frac{1}{\sqrt{2}} \left( 1 + \sqrt{1 - \frac{a^2}{M^2}} \right)^{1/2} \right]. \tag{4}$$

For nearly extremal Kerr BHs, the available energy stands up to 29% of a black hole's total mass energy. For SMBH with mass of $M = 10^9 M_\odot$, the rotational energy is of the order of $10^{74}$ eV, which makes these objects the largest energy reservoirs in the Universe. Therefore, it is important to search for the signatures of efficient energy extraction from these vast resources, both theoretically and observationally.

Many attempts have been made to harness the energy of rotating BHs with the first one proposed by Roger Penrose in 1969 in his famous process [11]. Since a test particle traveling inside the ergosphere of a rotating black hole may have negative energy relative to an observer at infinity, yet the locally measured energy remains positive, Penrose showed that the BH's rotational energy can be extracted through the fragmentation of test particles inside the ergosphere. If one of the pieces of an initial particle achieves negative energy and falls into a black hole, another one may escape from the ergosphere with energy greater than the initial particle's energy. However, the efficiency of the Penrose process (measured as the ratio of acquired to input energies) was restricted to a maximum of 21% [12,13].

In 1975, Ruffini and Wilson formulated an idea based on charge separation in a magnetized plasma accreting into a Kerr BH, through which the rotational energy of BH can be extracted [14]. Later in 1977, a similar mechanism based on a magnetized plasma dynamics powered by BH spin was published [15], which became known as the Blandford–Znajek mechanism (BZ). Currently, BZ is a commonly accepted process of acceleration of relativistic jets, which are observed in various BH systems. In the mid-1980s, the Penrose process was generalized to include the effects of electromagnetic fields surrounding BH [16,17]. In this mechanism, called the magnetic Penrose process (see a more recent review at [18]), the interacting particles were charged, which allowed one to obtain extraordinary efficiencies exceeding 100% [19]. Following these works, many other BH energy extraction mechanisms were formulated (see, for example, reviews [18,20–22]), including the very recent radiative Penrose process [23] and electric Penrose process [24]. The magnetic Penrose process (MPP) was revisited [18] and it was found that the MPP operates in three regimes of effectiveness, covering other different processes. The most efficient regime of MPP predicts an efficiency of energy extraction of the order of $10^{13}$%. This mechanism is currently the most efficient among the known processes of energy extraction from rotating BHs. Therefore, in this paper, we use this mechanism to constrain the acceleration capabilities of various BH candidates. It was already shown in [9] that the process can accelerate charged particles to ultra-high energy as large as $10^{21}$ eV when applied to SMBH of typical mass and magnetic field. We are going to generalize these results and derive the limiting energy of charged particles accelerated by various BH sources, including galactic stellar mass BH binaries.

### 2.2. Magnetosphere of Rotating BHs: Magnetic Field—BH Mass Relation

Black holes, both stellar and supermassive, are usually surrounded by accretion disks constituted from highly ionized plasma, which gives rise to the generation of magnetic fields due to electric currents floating in the plasma. In binary systems, BHs can also be immersed into the magnetic field of the companion star. If the companion is a neutron star or magnetar, the immersed field can be relatively strong. On the contrary, a hypothetical isolated black hole without sufficient plasma distribution in its vicinity will be immersed into external large-scale magnetic field, which may have galactic or extragalactic origin, although the strengths of such a magnetic field are relatively weak. Observations toward the measurements of magnetic fields around compact objects indicate that a typical magnetic field for stellar mass BHs (most of which are located in binary systems) is of the order of $10^8$ G, while for supermassive BH, the same is of the order of $10^4$ G [25,26].

Various observational measurements and estimates indicate the existence of an inverse mass dependence of magnetic fields around BHs. In Figure 1, we selected 8 galactic stellar mass BHs observed in X-ray binaries and 25 local SMBHs located mostly at the centers of AGNs (except Sgr A*, which is not active and located at the center of the Milky Way) and fitted their positions at the magnetic field–mass diagram by linear and quadratic functions. The observational data used in the figure are given in Table 1 for galactic BHs and in Table 2 for SMBHs. The best obtained fit for all sources (combining both stellar and supermassive BHs) gives the following relation:

$$\mathrm{Log}(B[G]) = -0.5\,\mathrm{Log}\left(\frac{M}{M_\odot}\right) + 7.7. \tag{5}$$

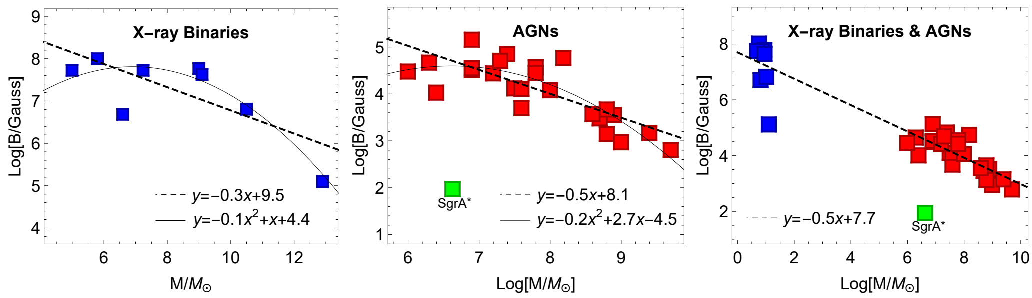


**Figure 1.** Positions of various BH candidates at the magnetic field–mass diagram. Blue squares denote the galactic stellar mass BHs observed in X-ray binaries, red squares the SMBH in AGNs, and the green square corresponds to Sgr A*, the galactic center SMBH. The data and references are given in Tables 1 and 2. Note the difference in the mass scales between the plots on the left (linear in mass) and other two (logarithmic). The fitting functions are seen as $y \equiv \mathrm{Log}B$, while $x$ is either $M$ (left plot) or Log $M$. All logarithms are common.

The function is shown as a dashed line on the right side plot of Figure 1. Although in order to define the magnetic field–mass dependence more precisely, one has to consider a larger number of sources, the results are similar to the previously obtained ones by [25,26]. It is interesting to note that according to these results, the observational estimate of magnetic field around Sgr A* at the center of our galaxy is rather weak, which complies with the fact that the galactic center is currently not active [27], in contrast to the selected SMBH sources presented in the figure.

One should note that any astrophysically relevant magnetic field is weak, meaning that its energy–momentum tensor has no effect on the BH metric [28]. One can easily prove it by simply comparing the magnetic field energy in a unit volume to the mass energy of a BH, which gives us $B_G = c^4/(G^{3/2}M) \sim 10^{19} M_\odot/M$. Since there is no evidence of the existence of magnetic fields of such orders in the vicinity of BHs, the spacetime metric remains safe, as well as the no-hair theorem hypothesis. On the other hand, while the magnetic field is weak for gravity, its influence on charged particles, such as electrons, protons and ions is non-negligible—it is rather enormous due to the effect of the Lorentz force. For example, the ratio of the Lorentz to gravitational forces acting on a proton moving around Sgr A* is of the order of

$$\frac{F_{\mathrm{Lorentz}}}{F_{\mathrm{grav.}}}\bigg|^{p^+}_{\mathrm{SgrA}^*} \approx 10^7 \left(\frac{q}{e}\right)\left(\frac{m}{m_{p+}}\right)^{-1}\left(\frac{B}{10\,\mathrm{G}}\right)\left(\frac{M}{4\times 10^6\, M_\odot}\right). \tag{6}$$

For an electron, this ratio is $\sim$2000 times greater. Thus, the magnetic field effects on the charged particle dynamics around BHs cannot be neglected [29].

While the strengths of magnetic fields around BHs can be estimated combining various measurements and models, the structures of the fields and their configurations are more challenging to identify. In the black hole vicinity, where gravity plays a leading role, one can use the natural assumption of stationarity and axial symmetry of the external magnetic field that is sharing the background symmetries of the Kerr metric spacetime. Let us choose the magnetic field to be asymptotically uniform so that the four-vector potential of electromagnetic field has two non-vanishing components [30]

$$A_t = aB\left(\frac{Mr}{\Sigma}\left(1+\cos^2\theta\right)-1\right), \tag{7}$$

$$A_\phi = \frac{B}{2}\left(r^2+a^2-\frac{2Mra^2}{\Sigma}\left(1+\cos^2\theta\right)\right)\sin^2\theta. \tag{8}$$

This solution was obtained by R. Wald in 1974 [30]. One can also mention other magnetic field configurations, such as the inclined magnetic field solution by J. Bičák and V. Janiš [31] and the dipole magnetic field of a current loop orbiting around rotating BH by J. Petterson [32], among others. As it was shown in [18], in the context of BH energy extraction, the field configuration plays a rather secondary role. However, since the charged particles escape along the magnetic field lines, the configurations with open field lines are more preferable.

A spinning BH in an external magnetic field induces an electric field component, resulting in a non-zero potential difference between the horizon and infinity. The induced electric field due to the frame-dragging effect having quadrupole structure and appearing in all configurations can be referred to as the BH charge [33–36], which is responsible for the high-energy acceleration of charged particles.

**Table 1.** CR acceleration capabilities of selected galactic BH candidates observed in X-ray BH binaries with measured masses $M$, spins $a = Jc/(GM^2)$, equipartition magnetic field strengths $B$ and predicted mean energies of proton $E_{p+}^{\mathrm{mean}}$ accelerated by the given corresponding source.

| Source | Refs. | $M/M_\odot$ | Spin $a$ | $\mathrm{Log}(B/1\,\mathrm{G})$ | $\mathrm{Log}\left(E_{p+}^{\mathrm{mean}}/1\,\mathrm{eV}\right)$ |
|---|---|---|---|---|---|
| GX 339-4 | [25,37] | $5.8 \pm 0.5$ | $0.92 \pm 0.06$ | $8.07 \pm 0.18$ | $15.7 \pm 0.2$ |
| V404 Cygni | [25,38] | $9.0 \pm 0.6$ | $0.97 \pm 0.02$ | $7.84 \pm 0.24$ | $15.6 \pm 0.4$ |
| XTE J1118+480 | [25,39] | $7.2 \pm 0.9$ | $0.66 \pm 0.02$ | $7.80 \pm 0.10$ | $15.7 \pm 0.2$ |
| A0620-00 | [25,40] | $6.6 \pm 0.3$ | $0.98 \pm 0.07$ | $6.76 \pm 0.06$ | $14.4 \pm 0.3$ |
| GRS 1915+105 | [41–44] | $12.9 \pm 2.4$ | $0.98 \pm 0.01$ | $5.17 \pm 0.83$ | $13.2 \pm 0.9$ |
| XTE J1650-500 | [45,46] | $5.0 \pm 2.0$ | $0.80 \pm 0.10$ | $7.80 \pm 0.20$ | $15.5 \pm 0.4$ |
| XTE J1550-564 | [44,47,48] | $9.1 \pm 0.6$ | $0.49 \pm 0.20$ | $\approx 7.70$ | $15.6 \pm 0.2$ |
| H 1743-322 | [49,50] | $10.5 \pm 3.1$ | $0.30 \pm 0.10$ | $\approx 6.88$ | $14.3 \pm 0.6$ |

**Table 2.** UHECR acceleration capabilities of selected SMBH candidates with measured masses $M$, distances $d$ (within about 100 Mpc), dimensionless spins $a = Jc/(GM^2)$, equipartition magnetic field strengths $B$ and predicted mean energies of proton $E_{p+}^{\rm mean}$ accelerated by a corresponding source.

| Source | d (Mpc) | $\mathrm{Log}(M/M_{\odot})$ | Spin $a$ | $\mathrm{Log}(B/1\,\mathrm{G})$ | $\mathrm{Log}\left(E_{p+}^{\rm mean}/1\,\mathrm{eV}\right)$ |
|---|---|---|---|---|---|
| Sgr A* | (GC) 0.008 | 6.63 | 0.6 | 2 | 15.64 |
| NGC 1052 | 19 | 8.19 | $\lesssim$1 | 4.8 | 20.11 |
| NGC 1068/M77 | 15 | 6.9 | $\lesssim$1 | 4.54 | 18.56 |
| NGC 1365 | 17 | 6.3 | $\lesssim$1 | 4.70 | 18.12 |
| NGC 2273 | 29 | 6.9 | 0.97 | 4.58 | 18.41 |
| NGC 2787 | 8 | 7.6 | $\lesssim$1 | 3.73 | 18.45 |
| NGC 3079 | 22 | 6.4 | $\lesssim$1 | 4.06 | 17.58 |
| NGC 3516 | 42 | 7.4 | 0.64 | 4.88 | 19.37 |
| NGC 3783 | 41 | 7.5 | 0.98 | 4.15 | 18.77 |
| NGC 3998 | 15 | 8.9 | 0.54 | 3.58 | 19.52 |
| NGC 4151 | 14 | 7.8 | 0.84 | 4.6 | 19.53 |
| NGC 4258/M106 | 8 | 7.6 | 0.38 | 4.14 | 18.65 |
| NGC 4261 | 32 | 8.7 | $\lesssim$1 | 3.51 | 19.33 |
| NGC 4374/M84 | 20 | 9 | 0.98 | 3 | 19.12 |
| NGC 4388 | 18 | 6.9 | 0.51 | 5.19 | 19.11 |
| NGC 4486/M87 | 17 | 9.7 | $\lesssim$1 | 2.84 | 19.66 |
| NGC 4579 | 18 | 8 | 0.82 | 4.11 | 19.23 |
| NGC 4594 | 11 | 8.8 | 0.6 | 3.18 | 19.05 |
| NGC 5033 | 20 | 7.2 | 0.68 | 4.47 | 18.77 |
| NGC 5194/M51 | 8 | 6.0 | 0.57 | 4.51 | 17.57 |
| MCG-6-30-15 | 33 | 7.3 | 0.98 | 4.74 | 19.16 |
| NGC 5548 | 75 | 7.8 | 0.58 | 4.48 | 19.34 |
| NGC 6251 | 102 | 8.8 | $\lesssim$1 | 3.70 | 19.62 |
| NGC 6500 | 43 | 8.6 | $\lesssim$1 | 3.60 | 19.32 |
| IC 1459 | 31 | 9.4 | $\lesssim$1 | 3.20 | 19.72 |

## 3. Black Hole Rotating in Magnetic Field as CR Accelerator

### 3.1. Generalized Formalism

Let us now consider the motion of a test charged particle with mass $m$ and charge $q$. For the particle, one can define two conserved quantities (energy and angular momentum), which are the components of the canonical four-momentum $P_\mu = mu_\mu + qA_\mu$:

$$E = -P_t = mu_t + qA_t, \quad L = P_\phi = mu_\phi + qA_\phi, \tag{9}$$

where $u^\mu$ is the particle's four velocity. Now, we consider the split of a particle $A$ into two charged fragments $B$ and $C$ in the black hole ergosphere at the equatorial plane. The conservation laws before and after split can be written as follows:

$$E_A = E_B + E_C, \quad L_A = L_B + L_C, \quad q_A = q_B + q_C, \quad m_A \geq m_B + m_C. \tag{10}$$

If one of the particles after split, e.g., particle $B$, attains negative energy, particle $C$ comes out with energy exceeding the energy of the incident particle $A$ at the expense of the rotational energy of the BH.

Skipping routine calculations that can be found in [18], we focus on the conditions, for which the energy extraction efficiency grows ultra high. We fix the plane of the motion of the incident particle $A$ to the equatorial plane $\theta = \pi/2$ and assume that the particle $A$ is neutral, splitting into two charged fragments. Then, the leading term for the energy of the escaping ionized particle takes the following simple form:

$$E_C \approx \frac{q_C}{m_A} A_t^{ion} E_A, \tag{11}$$

where $A_t^{ion}$ is the time component of the covariant form of the electromagnetic four potential calculated at the fragmentation point of the incident neutral particle $A$. Note that $A_t^{ion}$ is nonzero in the black hole vicinity due to the frame-dragging effect [30]. The energy in this mechanism can grow ultra-high under realistic conditions [9].

Since neutral particles may travel arbitrarily close to the event horizon without being affected by electromagnetic fields, ionization can occur extremely close to the black hole and take advantage of the strong gravity interactions. As a result, in addition to gravitational negative energy in the ergosphere, the charged fragment following the ionization of the neutral particle attains a very high Coulombic contribution to the energy. Initially charged particles in the plasma surrounding the BH are unable to use the Coulombic contribution. In Figure 2, we illustrate the numerical results of the process of ionization of a freely falling neutral particle and the resulting escape of an ionized particle (red curves) with higher energy than that of the neutral particle.

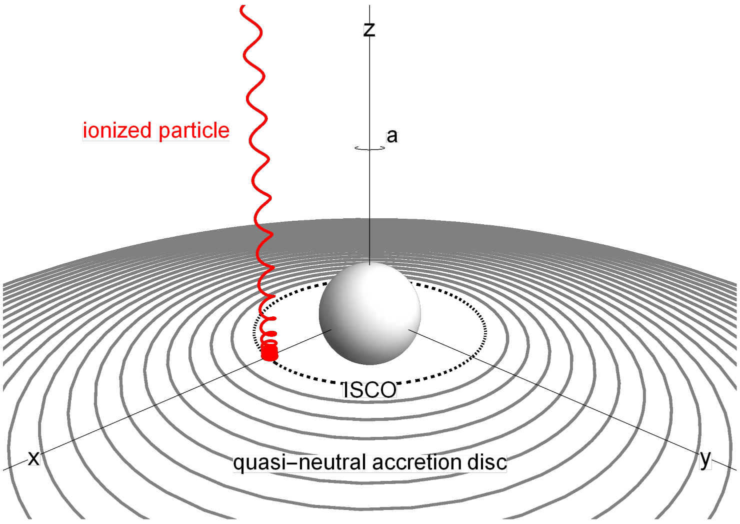


**Figure 2.** Schematic picture of the CR acceleration scenario based on the ionization of a neutral particle close to the innermost stable circular orbit (dashed circle) of rotating black hole. The trajectory is obtained numerically by integrating equations of motion in Kerr metric in the presence of external uniform magnetic field aligned along the rotation axis.

### *3.2. Mean Energy of Cosmic Rays Accelerated by Various BH Candidates*

In general, the magnetic field has a complex structure around the event horizon, but locally, at the splitting point, the field may be considered uniform [30]. In order to obtain the required estimates, let us consider the ionization of a freely falling neutral atom with atomic number $Z$, mass number $A$ and energy $E = m_A c^2 \sim A \times 10^9$ eV into a BH. The energies of escaping ionized particles from stellar mass and supermassive BHs [9] take the following values:

$$E_{\rm ion}^{\rm BH} \approx 10^{16}{\rm eV}\, \frac{Z}{A} \frac{B}{10^8{\rm G}} \frac{M}{10 M_\odot}, \tag{12}$$

$$E_{\rm ion}^{\rm SMBH} \approx 10^{20}{\rm eV}\, \frac{Z}{A} \frac{B}{10^4{\rm G}} \frac{M}{10^9 M_\odot}. \tag{13}$$

For $A = Z = 1$, e.g., in the process of the neutron beta decay, $n^0 \to p^+ + e^- + \bar{\nu}_e$, the energy of the escaping proton is of the order of $E_{p+} \approx 10^{16}$ eV for stellar mass BHs and $E_{p+} \approx 10^{20}$ eV for SMBHs. Here, we took the ionization point at $r_{ion} = r_g$, i.e., far enough from the horizon of rotating BH, so that the charged particles are able to escape from the inner regions. In astrophysically plausible conditions, the accelerated charged particle after ionization or fragmentation is more likely to be positively charged (proton or ion) since the induced BH charge has more likely a positive sign [30,33].

### 3.3. CR Propagation: GZK and Synchrotron Losses

Due to the GZK cutoff [3,4], there exists an upper bound on the distance from which the very high energy protons are capable of reaching the observer at Earth. This distance is predicted to be <100 Mpc [2], for the corresponding proton energy $5 \times 10^{19}$ eV. The discovery of UHECR events with energy larger than the GZK-cutoff limit raises issues about the origin, propagation, and composition of CRs at the highest energy. If UHECR particles with energy around $10^{20}$ eV are made up of heavier nucleons, the interaction of high-energy ions with intergalactic radiation causes nuclei to be excited, photodisintegrated, and fragmented into protons and neutrons due to internal resonances. This highlights the significance of GZK and photodisintegration events in UHECR propagation, which is taken into account in choosing potential extragalactic sources in Table 2. Moreover, the interaction of CRs with the BH environment (matter, photons and magnetic field) in the source region has to be also taken into account, due to the hot and dense plasma matter surrounding BHs. The interaction of CRs with matter bounds the possible directions of the particles' escape. Together with the magnetic field effects, this leads to the collimated emission of charged particles along the magnetic field lines, opening the equipotential surfaces and narrow funnel around the axis of BH rotation [20]. However, interactions of accelerated particles with photons in the source region can considerably influence the particle propagation. The losses of primary CRs due to the interaction with photons originated near the BH need to be determined, which we leave for future works. In addition, UHECRs interact with the magnetic field, causing synchrotron radiation. Although energy suppression due to electromagnetic radiation in galactic and intergalactic magnetic fields is small [51], UHECRs can lose a significant portion of their energies in the source regions, as we show below.

For ultra-relativistic charged particles, the presence of an external magnetic field and curvature of the spacetime leads to the non-trivial form of synchrotron radiation. A detailed study of the motion of a charged particle, taking into account the radiation–reaction force, can be found in [51], and the references therein. The dynamical equations take the following form:

$$\frac{Du^\mu}{d\tau} = \frac{q}{m} F^\mu{}_\nu u^\nu + \frac{2q^3}{3m^2}\left(\frac{DF^\alpha{}_\beta}{dx^\mu} u^\beta u^\mu + \frac{q}{m}\left(F^\alpha{}_\beta F^\beta{}_\mu + F_{\mu\nu} F^\nu{}_\sigma u^\sigma u^\alpha\right) u^\mu\right), \tag{14}$$

where $u_\alpha$ is normalized as $u^\alpha u_\alpha = -1$, and $F^\mu_\nu$ is the electromagnetic Faraday tensor. The time component of the Equation (14) leads to the time evolution of energy of the particle, due to synchrotron radiation loss [51]. The characteristic synchrotron radiation timescale is given by

$$\tau_{synchrotron} \approx \left(1 - \frac{2\,GM}{r\,c^2}\right)^{-1} \frac{3\,m^3 c^5}{2\,q^4 B^2}. \tag{15}$$

Note that Equation (15) is derived for an ultra-relativistic particle with the Lorentz factor $\gamma \gg 1$. The speed of the radiation losses decreases close to BH as the cooling time increases. It is important to note that the electron cooling timescale is $10^{10}$ times faster than for protons due to the cubic mass dependence in Equation (15). In Table 3, we show characteristic synchrotron radiation timescales for electrons, protons and iron nuclei for different values of magnetic field strength. Thus, the energy loss can be quite relevant, especially in the case of lighter particles, such as electrons.

CR passing through large distances inevitably interact with magnetic fields, which can vary from $10^{-5}$ G (Galactic or intergalactic) up to the strengths $10^4$ G up to $10^8$ G near their accelerating sources depending on the source type. Since the electron radiation timescale is ten orders of magnitude faster than that for protons, heavier CR constituents have a greater chance of overcoming the synchrotron radiation losses. However, if the magnetic field is too strong $\gg 10^4$ G, then synchrotron losses become dominant also for protons and ions. For example, in the case of neutron stars having typical magnetic fields of the order of $10^{12}$ G, the characteristic synchrotron radiation timescale for protons is of the order of $10^{-6}$ s. In this situation, high-energy CR particles would be able to escape the star only along the trajectories strictly parallel to the magnetic field lines, which can be possible only in very narrow cones at the polar cap regions, where magnetic field lines are straight and open to infinity. Such a collimation of accelerated particles requires fine-tuning of the dynamical parameters of the particle.

Therefore, taking into account the above given arguments, among the compact objects, BHs (both stellar and supermassive) seem more plausible candidates for high-energy CR accelerators.

**Table 3.** Characteristic synchrotron radiation timescales of ultra-relativistic electrons $\tau_e$, protons $\tau_p$ and iron nuclei $\tau_{\rm Fe}$ for different magnetic field values $B$.

| **B (Gauss)** | $10^{12}$ | $10^8$ | $10^4$ | 1 | $10^{-4}$ |
|---|---|---|---|---|---|
| $\tau_e$ **(s)** | $10^{-16}$ | $10^{-8}$ | 1 | $10^8$ | $10^{16}$ |
| $\tau_p$ **(s)** | $10^{-6}$ | $10^2$ | $10^{10}$ | $10^{18}$ | $10^{26}$ |
| $\tau_{\rm Fe}$ **(s)** | $10^{-5}$ | $10^3$ | $10^{11}$ | $10^{19}$ | $10^{27}$ |

## 4. Conclusions and Future Prospects

In this paper, we generalized the CR acceleration model proposed in [9] to a larger number of objects of two classes: stellar and supermassive BHs. The rotation of a BH in an external magnetic field leads to the induction of an electric field due the effect of the frame dragging and subsequent selective accretion and net charging of the black hole. The highest efficiency and subsequent acceleration are achieved in the process of decay of the initially neutral particle close to the BH into two or more charged fragments. In such cases, which include the processes of ionization, the energy of the charged fragment can be increased, due to the electromagnetic interaction between the particle and BH. Due to the co-rotation of the matter with the BH, the alignment of the magnetic field lines at the event horizon scales is usually governed by the BH spin. Therefore, a positive induced charge of the BH is plausible. As a result, the accelerated fragments after the decay of a neutral particle are likely positively charged. Negatively charged fragments are expected to eventually fall into the BH, leading to the decrease in the BH's angular momentum.

In Tables 1 and 2, we summarize the results of the current paper, providing constraints on the CR acceleration capabilities of selected stellar mass and supermassive BHs and their relevant parameters. Taking into account the GZK-cutoff limit, photodisintegration and synchrotron radiation losses, we calculated the mean energies of protons, which can be accelerated by the given source. For stellar mass BHs, we chose 8 galactic sources and for SMBHs 25 extragalactic sources within 100 Mpc. For stellar mass BHs, typically, the acceleration capabilities do not exceed $10^{16}$ eV, while for SMBHs in AGNs, they are of the order of $Z \times 10^{20}$ eV. Among the stellar mass X-ray binaries and AGNs, we also studied the acceleration capability of the galactic center SMBH, for which it was found that the proton energy coincides with the knee of the CR spectrum and can potentially contribute to its sharpness. This result is well in accord with the observations: the galactic center is currently not active, it has a relatively weak magnetic field (<100 G), and the observed CRs with energy above the knee are likely extragalactic.

Due to the strong tidal forces and hot environment in the vicinity of stellar mass BHs, the acceleration of CR ions heavier than protons is less likely in contrast to SMBH cases. Additionally, it is expected that primary CR protons accelerated by stellar mass BHs would lose significant parts of their energies in synchrotron radiation in the source regions due to stronger magnetic fields surrounding stellar mass BHs in comparison to SMBHs (see Table 3). In such cases, the direction of escape of the high-energy charged particles are preferred in the directions along the magnetic field lines. These all constrain the energy of primary CRs reaching the Earth, from galactic BHs to the values, which would normally not exceed the knee of the cosmic ray spectrum. In the case of SMBHs, unlike the jet acceleration models and due to the relatively weak magnetic fields, the direction of escape of ionized high-energy particles is expected to be more isotropic. Averaged over selected SMBH, the mean proton energy was found to be around $10^{19}$ eV. The existence of several sources at such energies can potentially contribute to the ankle of the CR spectrum, although the spectrum for particular SMBH is yet to be determined. Even though the presented model gives certain predictions on the parameters of BHs as CR sources, a more detailed study of the model is required to reproduce such CR observables as the flux, energy spectrum, composition, and spectral shape. These features of the model will be addressed in future publications.

The list of objects presented in Tables 1 and 2 is obviously not exhaustive, and has to be extended in the future by using more multi-wavelengths data related to the measurements of BH masses, spins and magnetic fields. Another direction of potential search is the experimental study of CR correlations and arrival directions being realized on different scales. Extreme conditions around BHs, especially of AGNs with SMBHs at their centers, increase the chances for the engagement of accelerated UHECRs in the production of the so-called CR ensembles (CRE)—a group of correlated CR events—including photons with a common primary interaction vertex or the same parent particle. From this prospect, the recently founded Cosmic Ray Extremely Distributed Observatory (CREDO) [52] might be useful in revealing the origin of these remarkable phenomena.

**Author Contributions:** Conceptualization, A.T.; methodology, A.T.; writing—original draft preparation, A.T.; writing—review and editing, M.K. and Z.S.; visualization, M.K. and A.T. All authors have read and agreed to the published version of the manuscript.

**Funding:** This research received no external funding.

**Institutional Review Board Statement:** Not applicable.

**Informed Consent Statement:** Not applicable.

**Data Availability Statement:** Not applicable.

**Acknowledgments:** The authors would like to acknowledge the Research Centre for Theoretical Physics and Astrophysics and Institute of Physics of Silesian University in Opava for the institutional support.

**Conflicts of Interest:** The authors declare no conflict of interest.

## Abbreviations

The following abbreviations are used in this manuscript:

| | |
|---|---|
| BH | Black hole |
| CR | Cosmic ray |
| AGNs | Active galactic nuclei |
| GBHs | Galactic black holes |
| SMBH | Supermassive black hole |
| UHECR | Ultrahigh-energy cosmic ray |
| CREDO | Cosmic Ray Extremely Distributed Observatory |
| $\mathrm{Log}(x)$ | $\mathrm{Log}_{10}(x)$ |

## References


1. Pierre Auger Collaboration. An Indication of Anisotropy in Arrival Directions of Ultra-high-energy Cosmic Rays through Comparison to the Flux Pattern of Extragalactic Gamma-Ray Sources. *Astrophys. J. Lett.* **2018**, *853*, L29. [CrossRef]
2. Stecker, F.W. Effect of Photomeson Production by the Universal Radiation Field on High-Energy Cosmic Rays. *Phys. Rev. Lett.* **1968**, *21*, 1016–1018. [CrossRef]
3. Greisen, K. End to the cosmic ray spectrum? *Phys. Rev. Lett.* **1966**, *16*, 748–750. [CrossRef]
4. Zatsepin, G.T.; Kuzmin, V.A. Upper limit of the spectrum of cosmic rays. *JETP Lett.* **1966**, *4*, 78–80.
5. Bykov, A.M.; Ellison, D.C.; Marcowith, A.; Osipov, S.M. Cosmic Ray Production in Supernovae. *Space Sci. Rev.* **2018**, *214*, 41. [CrossRef]
6. Nagar, N.M.; Matulich, J. Ultra-high energy cosmic rays detected by the Pierre Auger observatory. First direct evidence, and its implications, that a subset originate in nearby radiogalaxies. *Astron. Astrophys.* **2008**, *488*, 879–885. [CrossRef]
7. Garrappa, S.; Buson, S.; Franckowiak, A.; Shappee, B.J.; Beacom, J.F.; Dong, S.; Holoien, T.S.; Kochanek, C.S.; Prieto, J.L.; Stanek, K.Z.; et al. Investigation of Two Fermi-LAT Gamma-Ray Blazars Coincident with High-energy Neutrinos Detected by IceCube. *Astrophys. J.* **2019**, *880*, 103. [CrossRef]
8. Blandford, R.D. Acceleration of Ultra High Energy Cosmic Rays. *Phys. Scr. Vol. T* **2000**, *85*, 191–194. [CrossRef]
9. Tursunov, A.; Stuchlík, Z.; Kološ, M.; Dadhich, N.; Ahmedov, B. Supermassive Black Holes as Possible Sources of Ultrahigh-energy Cosmic Rays. *Astrophys. J.* **2020**, *895*, 14. [CrossRef]
10. Bardeen, J.M.; Carter, B.; Hawking, S.W. The four laws of black hole mechanics. *Commun. Math. Phys.* **1973**, *31*, 161–170. [CrossRef]
11. Penrose, R. Gravitational Collapse: The Role of General Relativity. *Nuovo Cimento Riv. Ser.* **1969**, *1*, 252.
12. Bardeen, J.M.; Press, W.H.; Teukolsky, S.A. Rotating Black Holes: Locally Nonrotating Frames, Energy Extraction, and Scalar Synchrotron Radiation. *Astrophys. J.* **1972**, *178*, 347–370. [CrossRef]
13. Wald, R.M. Energy Limits on the Penrose Process *Astrophys. J.* **1974**, *191*, 231–234. [CrossRef]
14. Ruffini, R.; Wilson, J.R. Relativistic magnetohydrodynamical effects of plasma accreting into a black hole. *Phys. Rev. D* **1975**, *12*, 2959–2962. [CrossRef]
15. Blandford, R.D.; Znajek, R.L. Electromagnetic extraction of energy from Kerr black holes. *Mon. Not. R. Astron. Soc.* **1977**, *179*, 433–456. [CrossRef]
16. Wagh, S.M.; Dhurandhar, S.V.; Dadhich, N. Revival of the Penrose process for astrophysical applications. *Astrophys. J.* **1985**, *290*, 12–14. [CrossRef]
17. Parthasarathy, S.; Wagh, S.M.; Dhurandhar, S.V.; Dadhich, N. High efficiency of the Penrose process of energy extraction from rotating black holes immersed in electromagnetic fields. *Astrophys. J.* **1986**, *307*, 38–46. [CrossRef]
18. Tursunov, A.; Dadhich, N. Fifty Years of Energy Extraction from Rotating Black Hole: Revisiting Magnetic Penrose Process. *Universe* **2019**, *5*, 125. [CrossRef]
19. Dadhich, N.; Tursunov, A.; Ahmedov, B.; Stuchlík, Z. The distinguishing signature of magnetic Penrose process. *Mon. Not. R. Astron. Soc.* **2018**, *478*, L89–L94. [CrossRef]
20. Stuchlík, Z.; Kološ, M.; Tursunov, A. Penrose Process: Its Variants and Astrophysical Applications. *Universe* **2021**, *7*, 416. [CrossRef]
21. Koide, S.; Baba, T. Causal Extraction of Black Hole Rotational Energy by Various Kinds of Electromagnetic Fields. *Astrophys. J.* **2014**, *792*, 88. [CrossRef]
22. Stuchlík, Z.; Kološ, M.; Kovář, J.; Slaný, P.; Tursunov, A. Influence of Cosmic Repulsion and Magnetic Fields on Accretion Disks Rotating around Kerr Black Holes. *Universe* **2020**, *6*, 26. [CrossRef]
23. Kološ, M.; Tursunov, A.; Stuchlík, Z. Radiative Penrose process: Energy gain by a single radiating charged particle in the ergosphere of rotating black hole. *Phys. Rev. D* **2021**, *103*, 024021. [CrossRef]
24. Tursunov, A.; Juraev, B.; Stuchlík, Z.; Kološ, M. Electric Penrose process: High-energy acceleration of ionized particles by nonrotating weakly charged black hole. *Phys. Rev. D* **2021**, *104*, 084099. [CrossRef]
25. Daly, R.A. Black Hole Spin and Accretion Disk Magnetic Field Strength Estimates for More Than 750 Active Galactic Nuclei and Multiple Galactic Black Holes. *Astrophys. J.* **2019**, *886*, 37. [CrossRef]
26. Piotrovich, M.Y.; Mikhailov, A.G.; Buliga, S.D.; Natsvlishvili, T.M. Determination of magnetic field strength on the event horizon of supermassive black holes in active galactic nuclei. *Mon. Not. R. Astron. Soc.* **2020**, *495*, 614–620. [CrossRef]
27. Eckart, A.; Hüttemann, A.; Kiefer, C.; Britzen, S.; Zajaček, M.; Lämmerzahl, C.; Stöckler, M.; Valencia-S, M.; Karas, V.; García-Marín, M. The Milky Way's Supermassive Black Hole: How Good a Case Is It? *Found. Phys.* **2017**, *47*, 553–624. [CrossRef]
28. Gal'tsov, D.V.; Petukhov, V.I. Black hole in an external magnetic field. *Sov. J. Exp. Theor. Phys.* **1978**, *47*, 419.
29. Tursunov, A.; Stuchlík, Z.; Kološ, M. Circular orbits and related quasiharmonic oscillatory motion of charged particles around weakly magnetized rotating black holes. *Phys. Rev. D* **2016**, *93*, 084012. [CrossRef]
30. Wald, R.M. Black hole in a uniform magnetic field. *Phys. Rev. D* **1974**, *10*, 1680–1685. [CrossRef]
31. Bicak, J.; Janis, V. Magnetic fluxes across black holes. *Mon. Not. R. Astron. Soc.* **1985**, *212*, 899–915. 212.4.899. [CrossRef]
32. Petterson, J.A. Magnetic field of a current loop around a Schwarzschild black hole. *Phys. Rev. D* **1974**, *10*, 3166–3170. [CrossRef]
33. Zajaček, M.; Tursunov, A.; Eckart, A.; Britzen, S. On the charge of the Galactic centre black hole. *Mon. Not. R. Astron. Soc.* **2018**, *480*, 4408–4423. [CrossRef]

34. Komissarov, S.S. Electrodynamics of black hole magnetospheres. *Mon. Not. R. Astron. Soc.* **2004**, *350*, 427–448. [CrossRef]
35. Punsly, B. *Black Hole Gravitohydromagnetics*; Springer Science & Business Media: Cham, Switzerland, 2001.
36. Beskin, V.S. REVIEWS OF TOPICAL PROBLEMS: Axisymmetric stationary flows in compact astrophysical objects. *Phys. Uspekhi* **1997**, *40*, 659–688. [CrossRef]
37. Hynes, R.I.; Steeghs, D.; Casares, J.; Charles, P.A.; O'Brien, K. Dynamical Evidence for a Black Hole in GX 339-4. *Astrophys. J. Lett.* **2003**, *583*, L95–L98. [CrossRef]
38. Khargharia, J.; Froning, C.S.; Robinson, E.L. Near-infrared Spectroscopy of Low-mass X-ray Binaries: Accretion Disk Contamination and Compact Object Mass Determination in V404 Cyg and Cen X-4. *Astrophys. J.* **2010**, *716*, 1105–1117. [CrossRef]
39. Cherepashchuk, A.M.; Katysheva, N.A.; Khruzina, T.S.; Shugarov, S.Y.; Tatarnikov, A.M.; Bogomazov, A.I. Optical, J and K light curves of XTE J1118 + 480 = KV UMa: The mass of the black hole and the spectrum of the non-stellar component. *Mon. Not. R. Astron. Soc.* **2019**, *490*, 3287–3308. [CrossRef]
40. Cantrell, A.G.; Bailyn, C.D.; Orosz, J.A.; McClintock, J.E.; Remillard, R.A.; Froning, C.S.; Neilsen, J.; Gelino, D.M.; Gou, L. The Inclination of the Soft X-ray Transient A0620-00 and the Mass of its Black Hole. *Astrophys. J.* **2010**, *710*, 1127–1141. [CrossRef]
41. Hurley, D.J.; Callanan, P.J.; Elebert, P.; Reynolds, M.T. The mass of the black hole in GRS 1915+105: New constraints from infrared spectroscopy. *Mon. Not. R. Astron. Soc.* **2013**, *430*, 1832–1838. [CrossRef]
42. Török, G.; Kotrlová, A.; Šrámková, E.; Stuchlík, Z. Confronting the models of 3:2 quasiperiodic oscillations with the rapid spin of the microquasar GRS 1915+105. *Astron. Astrophys.* **2011**, *531*, A59. [CrossRef]
43. Miller, J.M.; Raymond, J.; Fabian, A.C.; Gallo, E.; Kaastra, J.; Kallman, T.; King, A.L.; Proga, D.; Reynolds, C.S.; Zoghbi, A. The Accretion Disk Wind in the Black Hole GRS 1915+105. *Astrophys. J. Lett.* **2016**, *821*, L9. [CrossRef]
44. Kološ, M.; Tursunov, A.; Stuchlík, Z. Possible signature of the magnetic fields related to quasi-periodic oscillations observed in microquasars. *Eur. Phys. J. C* **2017**, *77*, 860. [CrossRef]
45. Orosz, J.A.; McClintock, J.E.; Remillard, R.A.; Corbel, S. Orbital Parameters for the Black Hole Binary XTE J1650-500. *Astrophys. J.* **2004**, *616*, 376–382. [CrossRef]
46. Slaný, P.; Stuchlík, Z. Mass estimate of the XTE J1650-500 black hole from the extended orbital resonance model for high-frequency QPOs. *Astron. Astrophys.* **2008**, *492*, 319–322. [CrossRef]
47. Chaty, S.; Dubus, G.; Raichoor, A. Near-infrared jet emission in the microquasar XTE J1550-564. *Astron. Astrophys.* **2011**, *529*, A3. [CrossRef]
48. Steiner, J.F.; Reis, R.C.; McClintock, J.E.; Narayan, R.; Remillard, R.A.; Orosz, J.A.; Gou, L.; Fabian, A.C.; Torres, M.A.P. The spin of the black hole microquasar XTE J1550-564 via the continuum-fitting and Fe-line methods. *Mon. Not. R. Astron. Soc.* **2011**, *416*, 941–958. [CrossRef]
49. Tursunov, A.A.; Kološ, M. Constraints on Mass, Spin and Magnetic Field of Microquasar H 1743-322 from Observations of QPOs. *Phys. At. Nucl.* **2018**, *81*, 279–282. [CrossRef]
50. Aneesha, U.; Mandal, S. Spectral and accretion evolution of H1743-322 during outbursts in RXTE era. *Astron. Astrophys.* **2020**, *637*, A47. [CrossRef]
51. Tursunov, A.; Kološ, M.; Stuchlík, Z.; Gal'tsov, D.V. Radiation Reaction of Charged Particles Orbiting a Magnetized Schwarzschild Black Hole. *Astrophys. J.* **2018**, *861*, 2. [CrossRef]
52. Homola, P.; Beznosko, D.; Bhatta, G.; Bibrzycki, Ł.; Borczyńska, M.; Bratek, Ł.; Budnev, N.; Burakowski, D.; Alvarez-Castillo, D.E.; Almeida Cheminant, K.; et al. Cosmic-Ray Extremely Distributed Observatory. *Symmetry* **2020**, *12*, 1835. [CrossRef]